

Nonstabilizerness Estimation using Graph Neural Networks

Vincenzo Lipardi¹, Domenica Dibenedetto¹,
Georgios Stamoulis¹, Evert van Nieuwenburg² and
Mark H.M. Winands¹

¹Department of Advanced Computing Sciences, Maastricht University, 6229 EN Maastricht, The Netherlands

² Leiden Institute of Advanced Computer Science, Leiden University, 2333 CA Leiden, The Netherlands

E-mail: vincenzo.lipardi@maastrichtuniversity.nl

Abstract. This article proposes a Graph Neural Network (GNN) approach to estimate nonstabilizerness in quantum circuits, measured by the stabilizer Rényi entropy (SRE). Nonstabilizerness is a fundamental resource for quantum advantage, and efficient SRE estimations are highly beneficial in practical applications. We address the nonstabilizerness estimation problem through three supervised learning formulations starting from easier classification tasks to the more challenging regression task. Experimental results show that the proposed GNN manages to capture meaningful features from the graph-based circuit representation, resulting in robust generalization performances achieved across diverse scenarios. In classification tasks, the GNN is trained on product states and generalizes on circuits evolved under Clifford operations, entangled states, and circuits with higher number of qubits. In the regression task, the GNN significantly improves the SRE estimation on out-of-distribution circuits with higher number of qubits and gate counts compared to previous work, for both random quantum circuits and structured circuits derived from the transverse-field Ising model. Moreover, the graph representation of quantum circuits naturally integrates hardware-specific information. Simulations on noisy quantum hardware highlight the potential of the proposed GNN to predict the SRE measured on quantum devices.

Keywords: Stabilizer Rényi Entropy, Graph Neural Networks, Nonstabilizerness Estimation, Random Quantum Circuits, Transverse Field Ising Model.

1. Introduction

Quantifying the computational resources required to achieve a quantum advantage is a main problem in quantum information theory. Nonstabilizerness, also known as *magic* [1, 2], emerges as a key resource for quantum advantage as it measures the deviation of a quantum state from the polynomial-time simulability in the framework of the Gottesman-Knill Theorem [3, 4]. This theorem states that any quantum computation that consists exclusively of Clifford operations can be perfectly simulated in

polynomial time by a classical machine. However, preparing a generic quantum state in the full Hilbert space requires resources beyond the Clifford group, since a universal gate set cannot be constructed using Clifford gates alone. The amount of these non-Clifford resources is referred to as nonstabilizerness.

To rigorously capture the effect of non-Clifford operations in quantum computations, several measures of nonstabilizerness have been proposed. Examples include negative quasi-probability [5], robustness of magic [6, 7], stabilizer nullity [8], Bell magic [9], and stabilizer Rényi entropies [10, 11]. Among these measures, we focus on the Stabilizer Rényi Entropy (SRE) [10] for two main reasons. First, SRE offers favorable computational properties [10–12], especially when compared to alternative measures that require costly optimization procedures [5–7]. Second, SRE is particularly suitable for experiments on real quantum devices [13, 14]. However, in the general case, the computational time required to calculate the SRE of a quantum state scales exponentially in the number of qubits [10]. Tensor Network (TN) methods are currently the most widely adopted approach to calculate SRE for quantum states [15–19]. Although TN methods offer a theoretical framework with polynomial scaling, they are practically limited to low bond dimension, which restricts the class of quantum states that can be efficiently represented. Recently, Neural Quantum States [20] have been proposed as a promising alternative to overcome these limitations by flexibly approximating quantum states with high entanglement. Motivated by previous research in machine learning applications to quantum technology [21–23], learning-based approaches have recently been proposed for trading off online computational cost with approximate nonstabilizerness estimation. On the one hand, in the restricted case of the stabilizer state classification, where the task is to distinguish between stabilizer and magic states [24], Convolutional Neural Networks achieve predictions that are robust under the Clifford group. On the other hand, classical machine learning approaches trained on tabular data achieve accurate estimation of SRE, but with limited generalization performances [25].

In this article, we formulate the nonstabilizerness estimation as a graph-level prediction task and propose a Graph Neural Network (GNN) [26] approach to bridge the gap between the bond dimension-limited TN methods and the limited performances of machine learning models. We test the performance of the proposed GNN approach through three different formulations of nonstabilizerness estimation with increasing difficulty by exploiting the capabilities of GNN to capture meaningful features in the graph-based circuit representation.

The three main contributions of the article are as follows.

- (i) We propose a GNN approach for the nonstabilizerness estimation problem, that exhibits higher generalization capabilities to larger quantum circuits, in terms of number of qubits and gate counts, and to unseen entanglement, compared to previous works [24, 25]. The experimental results highlight the positive impact of representing quantum circuits as graphs, which enables the model to effectively capture their intrinsic structural properties.

- (ii) We have generated and released a comprehensive dataset of quantum circuits tailored to address the nonstabilizerness estimation problem in the supervised learning setting [27]. The dataset contains a total of 1686000 quantum circuits designed to span a broad range of number of qubits, entanglement and SRE values. The dataset is structured to address the problem in three different formulations of increasing difficulty, including both classification and regression tasks. We expect this dataset to foster progress in the development and benchmarking of machine learning methods for nonstabilizerness estimation.
- (iii) We show the proposed GNN model is well-suited to predict the SRE measured on real quantum devices, as the graph-based representation can also encode the hardware specifics.

This article is structured as follows. Section 2 introduces the nonstabilizerness estimation problem. Section 3 discusses related work in the field of machine learning. Section 4 describes the data generation procedure and details the rationale behind its design. Section 5 describes the architecture and implementation details of the proposed GNN model. Section 6 presents the experimental setup and discusses the results. Section 7 summarizes the main findings of this research study, highlighting the strengths and limitations of the proposed model and outlining promising directions for future research.

2. Background

This section introduces the stabilizer formalism in Section 2.1, defines the SRE and describes the main challenges in its estimation in Section 2.2, and concludes with the problem formulations of the nonstabilizerness estimation problem presented in Section 2.3.

2.1. Stabilizer States

Let us consider an n -qubit quantum state and let $U(n)$ be the group of unitary operators on the Hilbert space $\mathcal{H} = (\mathbb{C}^2)^{\otimes n}$. We define the Pauli group $\tilde{\mathcal{P}}_n$ acting on \mathcal{H} as the set of all possible Pauli strings \mathcal{P}_n taken with multiplicative factors ± 1 and $\pm i$, and the Clifford group $\mathcal{C}(n) \subset U(n)$ as the normalizer of the Pauli group [28]:

$$\tilde{\mathcal{P}}_n = \{ \{ \pm 1, \pm i \} \times \mathcal{P}_n \}, \quad (1)$$

$$\mathcal{C}(n) = \{ C \in U(n) \mid \forall P \in \tilde{\mathcal{P}}_n, CPC^\dagger = P' \in \tilde{\mathcal{P}}_n \}. \quad (2)$$

Let us recall that a Pauli string is a tensor product of Pauli matrices, each acting on a different qubit of an n -qubit system: $\mathcal{P}_n = \{ \sigma_0, \sigma_1, \sigma_2, \sigma_3 \}^{\otimes n}$. $\tilde{\mathcal{P}}_n$ and $\mathcal{C}(n)$ are groups under the operation of matrix multiplication. The set of gates consisting of the CNOT gate, the Hadamard gate H, and the phase gate S is a generator of the Clifford group

$\mathcal{C}(n)$. Let $|b\rangle$ be any computational basis vector of \mathcal{H} . We can define the set of stabilizer states as the full Clifford orbit of $|b\rangle$ [28]:

$$\text{STAB} = \{C |b\rangle \mid C \in \mathcal{C}(n)\}. \quad (3)$$

As proved by the Gottesman-Knill Theorem [3], stabilizer states can be perfectly simulated by a classical computer in polynomial time. As a consequence, quantum computations restricted to stabilizer states and Clifford gates do not provide any computational advantage over the classical counterpart. Because the set of stabilizer states is closed under Clifford operations, and a universal quantum gate set cannot be constructed from Clifford gates alone, the preparation of a generic state in the Hilbert space requires resources beyond the Clifford group. The amount of such non-Clifford resources is referred to as the *nonstabilizerness* of the state.

Since it is possible to prepare fully-entangled quantum states that can be efficiently simulated on a classical computer [4, 28], entanglement is not the only resource to consider in the quest for quantum advantage. Nonstabilizerness, also known as *magic*, plays a fundamental role in assessing quantum advantage [1–3], and, as such, it is important to define a measure for it. A measure of nonstabilizerness should be a nonstabilizer monotone [11], invariant under Clifford operations, and ideally efficiently computable for practical applications.

A measure of nonstabilizerness is a positive scalar function $X : \mathcal{H} \rightarrow \mathbb{R}_+$ defined on the Hilbert space \mathcal{H} that fulfills three conditions: it evaluates to zero all and only the stabilizer states ($X(|\psi\rangle) = 0$ iff $|\psi\rangle \in \text{STAB}$), it is invariant under Clifford operations (for every $C \in \mathcal{C}(n)$, $X(|\psi\rangle) = X(C|\psi\rangle)$), and finally the additivity (for any $|\psi_1\rangle, |\psi_2\rangle \in \mathcal{H}$, $X(|\psi_1\rangle \otimes |\psi_2\rangle) = X(|\psi_1\rangle) + X(|\psi_2\rangle)$).

The first measures of nonstabilizerness that have been proposed involve optimization procedures [5–7], which come with high computational cost. Then, more tractable measures have been introduced, such as stabilizer nullity [8], Bell magic [9], and stabilizer Rényi entropies [10]. In this article, we focus on the stabilizer Rényi entropy (SRE) [10] due to its favorable computational properties [12, 15, 17–19], especially when compared to alternative measures that require costly optimization procedures [5–7], and its practical suitability for experimental measurements on quantum hardware [13, 14].

2.2. Stabilizer Rényi Entropy

For a pure n -qubit quantum state ρ , the *Stabilizer Rényi Entropy* (SRE) [10] of order α (also called Rényi index) is defined as:

$$M_\alpha(\rho) = \frac{1}{1-\alpha} \ln \sum_{P \in \mathcal{P}_n} \Xi_P^\alpha(\rho) - \ln(2^n) \quad (4)$$

where $\Xi_P(\rho) = \frac{1}{2^n} \text{Tr}(\rho P)^2$ and \mathcal{P}_n denotes the set of n -qubit Pauli strings. For Rényi index $\alpha \geq 2$, the M_α fulfills all the requirements of a proper measure of nonstabilizerness [9, 11]. In this article, we fix the index to the commonly used $\alpha = 2$ [11], and we will refer to SRE simply as M_2 .

Methods based on Matrix Product States [15, 16, 18, 19], and more in general Tensor Networks, offer a framework to compute M_2 efficiently in the number of qubits but in running time that depends exponentially on the bond dimensions. Then, these methods represent a powerful theoretical framework, but with practical limitations to low bond dimensions [17]. To overcome those limitations, recent advances have been made towards efficient M_2 computations using Neural Quantum States [20].

In the general case, the computational cost to compute M_2 of a quantum state using the Equation 4 grows exponentially with respect to the number of qubits n [10], as it requires estimating 4^n expectation values, corresponding to all possible combinations of Pauli strings.

2.3. Problem Formulation

In this section, we define three formulations of the nonstabilizerness estimation problem on quantum circuits, with the goal of providing tasks of increasing difficulty that can serve as benchmarks for our study and future research. The first is a classification task aimed at distinguishing quantum circuits that prepare stabilizer states from those that prepare magic states. This formulation relies uniquely on the definition of stabilizer states provided in Section 3 and it is therefore independent from all measures of nonstabilizerness, including M_2 . We refer to this task as the stabilizer state classification. The second is a classification task based on SRE [10], where the goal is to distinguish between quantum circuits with low and high M_2 values. The difficulty of this task is parameterized by the M_2 threshold, which determines the boundary between low- M_2 and high- M_2 quantum circuits. We refer to this task as the SRE-based classification. Finally, the third formulation is a regression task, where the goal is to estimate the degree of nonstabilizerness of a quantum circuit by predicting its positive real-valued M_2 . We refer to this task as the SRE estimation.

We emphasize that our formulation targets nonstabilizerness estimation at the circuit level, rather than at the level of quantum states. As a consequence, it does not require any form of quantum state tomography and relies uniquely on the circuit-based quantum circuit representation. On the one hand, the circuit-based formulation offers significant advantages for applications that are inherently defined within the circuit-model paradigm of quantum computing. An example are Variational Quantum Algorithms [29], whose link to M_2 has been recently discussed in [30]. On the other hand, the circuit-based formulation is not directly applicable to scenarios where the M_2 must be evaluated on unknown quantum states, for which a corresponding circuit is generally unavailable.

The stabilizer state classification, particularly relevant in the context discussed in [24], becomes efficiently solvable in its matrix or circuit formulation [31]. Differently from the stabilizer state classification, the SRE-based classification and the SRE estimation both involve evaluating the contribution of each gate and its parameters to the overall circuit M_2 , depending on their positions, which is generally hard as discussed

in Section 2.2. The SRE-based classification is not only computationally difficult but also physically relevant. In experiments on real quantum hardware, quantum noise can affect the measured M_2 values depending on both the circuit structure and the hardware specifics. By setting an appropriate threshold close to zero, the SRE-based classification can be used to identify stabilizer states in the presence of quantum noise. Lastly, the SRE estimation is the more general and challenging formulation of the nonstabilizerness estimation problem.

3. Related Work

In the last decade, different review articles have emphasized the growing influence of machine learning in the physical sciences, see for example [21] and the reference therein, particularly within the rapidly evolving field of quantum technologies [22, 23].

In quantum computing, particular efforts have been made in tackling problems such as fidelity estimation [32–35], quantum compiling [36–40], ground-state energy estimation in many-body quantum systems [41], quantum error mitigation [42], quantum circuit expressibility estimation [43]. Following this research line, supervised learning approaches have been recently proposed to estimate the nonstabilizerness of quantum states [24, 25]. The first is a Convolutional Neural Network (CNN) approach proposed to distinguish between stabilizer and magic states [24]. In this work, the authors construct a balanced dataset of stabilizer and magic states restricted to product states of fixed size, with 18 qubits. Each state is represented by a $\mathcal{N} \times n$ binary matrix, where each row corresponds to a single-shot measurement outcome in the computational basis. This matrix is then converted into an image by assigning white pixels to zeros and black pixels to ones, enabling the use of CNN architectures. The CNN model achieves promising results, including predictions that are robust under the Clifford group, which means good generalization capabilities on entangled states. However, the CNN approach is limited to the stabilizer state classification problem and to fixed size of quantum states, because the number of qubits affects the size of the images. The second approach extended the nonstabilizerness estimation problem to a regression task for the supervised machine learning setting [25]. For this purpose, they use the M_2 as a measure of nonstabilizerness for quantum circuits. In the general case, computing M_2 of quantum states scales exponentially with the qubit number. The authors tackle the SRE estimation problem with different machine learning models, including Random Forest Regressor and Support Vector Regressor, providing a study on various tabular classical representations of quantum circuits, including circuit-level feature and expectation values of 1 and 2-local observables calculated using classical shadows [44]. The Support Vector Regressor (SVR) trained on feature vectors encoding the gate counts achieve the best performance. Although this approach showed promising experimental results to trade off online computational cost for approximate M_2 with machine learning, the models exhibit limited generalization capabilities to unseen larger circuits, in terms of both number of qubits and total gate count.

In this article, we advance beyond both the CNN and SVR approaches by proposing a Graph Neural Network (GNN) approach for nonstabilizerness estimation. Our method naturally accommodates both classification and regression formulations of the problem, while offering improved generalization capabilities compared to previous works [24, 25]. It is important to note that, in general, more complex models such as GNNs do not necessarily guarantee better performance. For example, in a recent study on supervised machine learning approaches to quantum error mitigation, Random Forests were shown to outperform other models, including GNNs [42]. The choice of data representations and model architectures is often task-dependent, and the design of the appropriate combination of features and models facilitate the learning of relevant properties and ensure robust generalization performance.

4. Data Generation

We generate a dataset divided into three main subsets, each tailored to one of the problem formulations introduced in Section 2.3.

Section 4.1 discusses the procedure to generate the data for the stabilizer state classification problem, where models are trained to distinguish between stabilizer and magic states. Section 4.2 details the post-processing applied to the previous dataset to address the SRE-based classification. Section 4.3 discusses the data generated for the SRE estimation problem, where models are trained to predict the positive real-valued M_2 of quantum circuits.

4.1. Data for Stabilizer State Classification

This section describes in detail the data generation procedure for the stabilizer state classification and an analysis to show the variety of the circuits designed across the number of qubits, entanglement and M_2 values. Furthermore, Section 6.1 presents the experimental results obtained on this benchmark problem.

It is important to note that, while the stabilizer state classification is an interesting task in the measurement-based representation, it becomes a trivial problem in our circuit-based formulation [31]. The primary goal of this section is therefore to introduce a well-defined and publicly available dataset for stabilizer state classification, which can serve as a benchmark for evaluating and comparing machine learning models under different generalization scenarios. Unlike previous work [24], where stabilizer and magic states exhibit clear separability in terms of their M_2 values, our proposed procedure ensures the generation of magic states spanning a broad range of M_2 values, including low- M_2 states that are more challenging to classify.

The stabilizer state classification problem has been previously investigated in the supervised learning setting [24]. However, performing our experiments on exactly the same dataset was not possible for two main reasons. First, the dataset itself is not available. Second, the data generation procedure was stochastic, and without access to

the original random seeds or generation metadata, identical reproduction could not be guaranteed. Nevertheless, the original authors provided all the necessary information to replicate and adapt their procedure in our circuit-based problem formulation.

The dataset for stabilizer state classification is constructed to formulate a circuit-level classification problem, where quantum circuits are labeled according to the quantum states they prepare, specifically distinguishing between stabilizer and magic states. Stabilizer states are assigned the label 0, while magic states are assigned the label 1. All circuits prepare n -qubit states, initialized as $|0\rangle^{\otimes n}$, where the number of qubits n spans the range from 2 to 25. The dataset consists of three main subsets, differing by the circuit composition and degree of entanglement:

- **Product States (PS):** quantum circuits composed only of single-qubit rotations gates: **RX**, **RY**, and **RZ**.
- **Clifford-evolved States (CS):** for each circuit in PS we generate 25 new circuits by evolving it under Clifford gates, uniformly sampled from the Clifford generator (**H**, **S**, **CNOT**). The Clifford gates are appended sequentially at the end of the product-state circuit. Each of the new circuits has a progressively higher number of new Clifford gates, referred as Clifford depth, from 1 to 25.
- **Entangled States (ES):** for each circuit in PS we generate one new circuit injected with a number of **CNOT** gates uniformly sampled between 1 and 20 and randomly placed throughout the circuit. The placement of each **CNOT** gate involves the random selection of two qubits to act as control and target, respectively. To ensure a non-trivial entangling structure, qubits that have not yet been acted upon by any gate are excluded from being selected as control qubits.

Note that, since PS is balanced between the two labels and because nonstabilizerness is invariant under Clifford, CS and ES are also balanced. Furthermore, by construction, the circuits in CS preserve part of the structure of the circuits in PS, while the circuits in ES may result in strongly different quantum circuit structures due to the random

Table 1: Overview of the dataset for stabilizer state classification.

Dataset	# Circuits	# Qubits	Label	SRE
PS 18	15000	18	Balanced	Computed per qubit
CS 18	375000	18	Inherited by PS 18	Inherited by PS 18
ES 18	15000	18	Inherited by PS 18	-
PS 2-25	33000	2–25	Balanced	Computed per qubit
CS 2-25	825000	2–25	Inherited by PS 2-25	Inherited by PS 2-25
ES 2-25	33000	2–25	Inherited by PS 2-25	-

placement of CNOT gates rather than their sequential appending. The computation of M_2 for circuits in PS can be easily performed by leveraging its additivity and compute M_2 as the sum of the M_2 computed per each qubit. Although CS inherits the M_2 values from the PS subset, the ES subset does not, since the contribution of each gate to the overall M_2 can change after the random CNOT injections, in the general case.

We generate two datasets, both including all three circuit type. The first is with a fixed number of qubit ($n = 18$), which is generated with the same size of the dataset used in [24], in order to have a fair comparison between our GNN and CNN. The second dataset instead enables more general experiments including quantum circuits with number of qubits ranging from 2 to 25. A schematic summary of the dataset for stabilizer state classification is provided in Table 1.

Each circuit is assigned a total number of gates G , uniformly sampled in $[10, 100]$. Stabilizer states are generated by applying gates randomly selected from the set of Clifford single-qubit rotations, while magic states involve single-qubit rotation gates with both Clifford angles and random angles, which inject magic into the circuits. For stabilizer states, each gate is chosen randomly among the set of allowed Clifford gates:

$$\mathcal{S}_S = \left\{ \text{RX}(\theta), \text{RY}(\theta), \text{RZ}(\theta) \mid \theta \in \left\{ \pm\frac{\pi}{2}, \pm\pi, \pm\frac{3\pi}{2} \right\} \right\} \cup \{ \text{H}, \text{S} \},$$

where the Hadamard gate and Phase gate are expressed in terms of rotation gates: $\text{H} = \text{RY}(\frac{\pi}{2})\text{RZ}(\pi)$ and $\text{S} = \text{RZ}(\frac{\pi}{2})$. For magic states, each gate is chosen from an extended gate set that includes both Clifford gates and single-qubit rotations with random angles:

$$\mathcal{S}_M = \mathcal{S}_S \cup \{ \text{RX}(\theta), \text{RY}(\theta), \text{RZ}(\theta) \mid \theta \in (0, 2\pi) \}.$$

Each magic states is assigned a ratio r_M of magic gates over the total number of gates uniformly sampled between 0.3 and 1, so that each magic circuit contains approximately

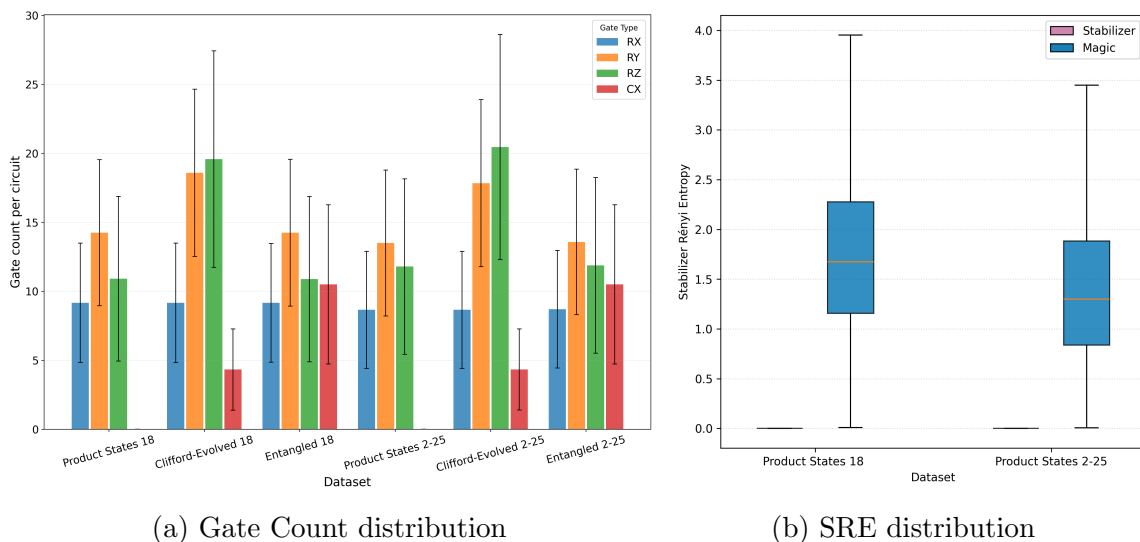


Figure 1: Overview of the quantum circuit composition in the dataset designed for the stabilizer state classification problem and the respective M_2 values.

$r_M \cdot G$ gates with random angles, effectively injecting varying degrees of nonstabilizerness into the circuit.

The presence of CS circuits in the dataset allows to investigate the generalization capabilities of the models to unseen entangled states, while keeping the same labels and M_2 values, in line with the procedure used in [24]. The Entangled States (ES) subset, on the other hand, enables a further step in this analysis by testing model performance on circuits characterized by substantially different structural patterns and, in general, a higher degree of entanglement. Figure 1 shows the heterogeneous quantum circuit dataset generated with our procedure, spanning a broad range of qubit number, circuit depth, circuit structure, entanglement and M_2 . Figure 1a illustrates the diversity of quantum circuits across the three different types in terms of gate counts and M_2 . It is important to note that our procedure generates also quantum circuits with significantly low M_2 values. For instance, in the case of 18-qubit circuits, the minimum M_2 value obtained in our dataset is 0.01, compared to 1.80 reported in [24]. Moreover, in the dataset PS 2-25, we observe a minimum M_2 value of 0.006, see Figure 1b. This is relevant, as the performance of machine learning models on the stabilizer state classification problem is typically correlated with the density of M_2 in the number of qubits n : $m_2 = \frac{M_2}{n}$. Models tend to achieve higher accuracy for states with higher m_2 , because of the increased separability of the magic states from the stabilizer states. This effect is also shown in the experimental results discussed in [24] and further confirmed by our own results obtained using graph neural networks (GNNs).

From a geometric perspective, stabilizer states form a discrete subset of the Hilbert space, i.e., the states reachable via the Clifford group acting on the computational basis. On the other hand, magic states lie outside this subset, covering regions of the Hilbert space not accessible through Clifford operations alone. The stochastic mixing of Clifford and non-Clifford gates thus corresponds to sampling points with varying distances from the set of stabilizer states, parameterizing to a certain extent the degree of magic in the resulting quantum states.

4.2. Data for SRE-based Classification

The datasets used for the SRE-based classification task derive from those introduced in the previous section for the stabilizer state classification.

All stabilizer states are removed from the original dataset, leaving only the quantum circuits labeled as magic states (with label one). Subsequently, the median of the M_2 values of the remaining circuits is computed and taken as the threshold M_2 to distinguish between circuits with low and high M_2 . This procedure makes the classification task particularly challenging, as the median corresponds to a region densely populated by quantum circuits with similar M_2 values. The violin plots in Figure 2 illustrates the distribution of M_2 values across the product-state datasets. The horizontal lines in the plot represent the median M_2 value for each dataset shown along the x-axis. As expected, quantum circuits with qubit numbers between 2 and 10 exhibit a narrower

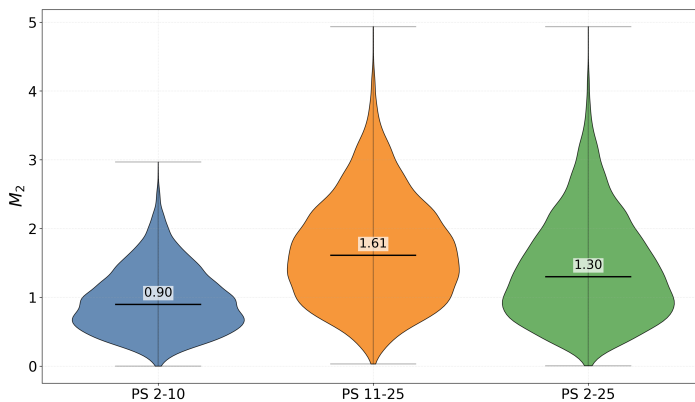


Figure 2: M_2 value distribution in datasets of product states.

range of M_2 values compared to circuits with qubit numbers between 11 and 25.

We note that by choosing the median as the threshold M_2 value in our dataset we ensure that is balanced between the two labels: low- M_2 and high- M_2 . However, the threshold choice is a way to parametrizes the difficulty of the classification task. In particular, for low M_2 threshold the SRE-based classification becomes a physics-motivated problem where the goal is to distinguish between stabilizer and magic states on a real quantum hardware. In this case, the threshold will respresent an indication of the quantum noise impact on the M_2 value of the stabilizer states.

4.3. Data for Stabilizer Rényi Entropy Estimation

The procedure used to generate the dataset for the regression formulation of the SRE estimation problem follows the approach described in [25], and reported in the following. In addition, we extend the dataset to noisy quantum simulations to investigate the effect of quantum noise on the performance of our model.

The dataset comprises two classes of quantum circuits, both defined for systems with a number of qubits n ranging from 2 to 6. The first class includes 250000 random quantum circuits (unstructured), 50000 for each value of n , and is hereafter referred to as the RQC dataset. The second class includes 25000 quantum circuits based on the Trotterized dynamics of the one-dimensional transverse-field Ising model (structured), 5000 for each value of n , hereafter referred to as the TIM dataset. All circuits are labeled with their M_2 value, computed from Equation 4. Each circuit is associated with two labels: the first corresponds to the M_2 obtained from noiseless simulations using a statevector simulator, and the second to the M_2 obtained from noisy simulations emulating the `Fake0s1o` backend of IBM Quantum. This dual labeling enables a systematic analysis of the impact of quantum noise on the GNN model performance.

These datasets are designed to be representative of typical circuits used in applications for NISQ devices [45], covering a wide range of M_2 values. The variety of quantum circuit structures included in the dataset is crucial for studying the generality and robustness of our approach. On the one hand, random quantum circuits provide

Table 2: Overview of the dataset for the SRE estimation problem.

Dataset	# Circuits	# Qubits	Depth	Extrapolation
RQC	250000	2–6	1–100	Qubits and Gate count
RQC Noisy	100000	2–6	1–80	Qubits and Gate count
TIM	25000	2–6	1–5	Qubits and Trotter steps
TIM Noisy	15000	2–6	1–5	Qubits and Trotter steps

a general and unstructured benchmark, as they are not linked to any specific problem domain. On the other hand, the transverse-field Ising model serves as a well-established benchmark in quantum machine learning, owing to its fundamental role in condensed matter physics, statistical mechanics, and quantum information. Moreover, the behavior of the SRE in the transverse-field Ising spin chain has been extensively investigated [46].

Table 2 provides a schematic overview of the datasets used for the SRE estimation problem. Figure 3 illustrates the M_2 value distribution under noiseless simulations for the RQC and TIM datasets. Specifically, Figures 3a and 3b show the M_2 distributions of quantum circuits grouped by qubit count, with their average values indicated by dashed vertical lines, for the RQC and TIM datasets, respectively. Figures 3c and 3d presents the average M_2 values, together with their standard deviations (shaded regions), for quantum circuits grouped by qubit number as a function of circuit depth. On the other hand, Figure 4 shows the corresponding distributions obtained from noisy simulations in comparison to the noiseless case. Figures 4a and 4b demonstrate that noisy quantum simulations have a stronger impact on the TIM dataset than on the RQC dataset: on average, the M_2 values in the TIM dataset shift more towards higher values, and the overall distributions become more stretched.

In the RQC dataset, once we fix the number of qubits n , the circuits are generated by sampling the number of gates uniformly from the range $G = [0, 100]$. Starting with an empty quantum circuit, gates are sequentially added, each randomly picked from a universal gate set comprising the CNOT gate and the three single-qubit rotation gates: **RX**, **RY**, **RZ**. In the TIM dataset, each quantum circuit represents a discrete-time approximation of the transverse-field Ising hamiltonian on a one-dimensional chain with nearest-neighbor interactions:

$$H = -J \sum_{i=1}^{n-1} Z_i Z_{i+1} - h \sum_{i=1}^n X_i,$$

where Z_i and X_i are Pauli operators acting on qubit i , J denotes the interaction strength, and h the transverse-field strength. The time-evolution operator $U(t) = e^{-iHt}$ is simulated using a first-order Trotter–Suzuki decomposition [28]. Each Trotter step is constructed as a sequence of quantum gates: the two-qubit interaction $e^{-i\theta Z_i Z_{i+1}}$, with

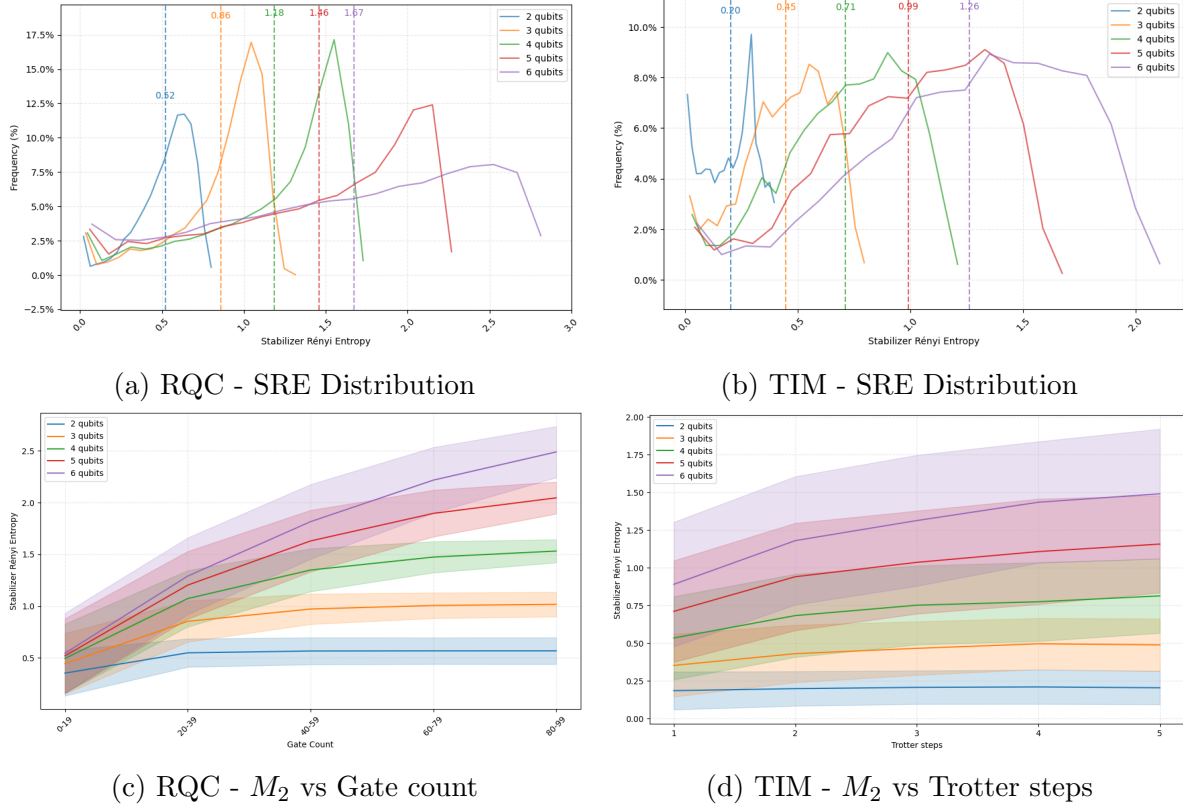


Figure 3: Overview of the distribution of the M_2 values across the quantum circuits in the dataset designed for the SRE estimation problem.

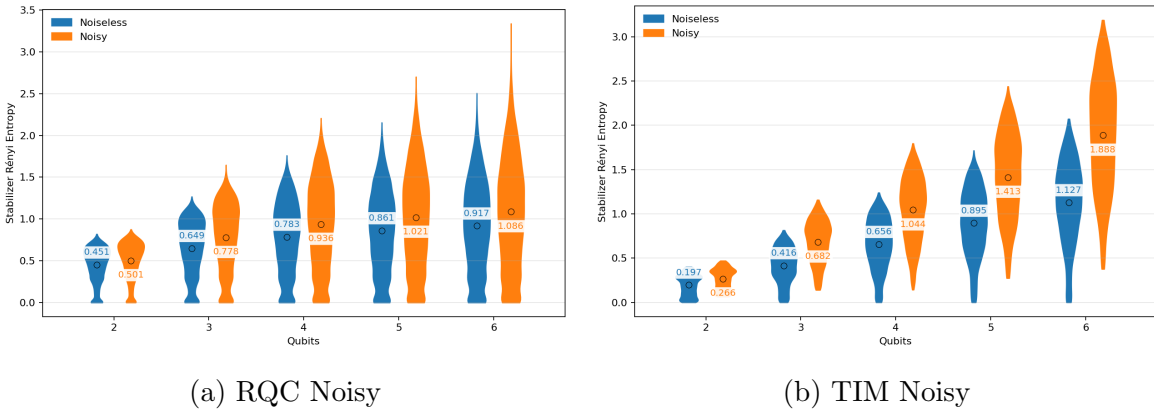


Figure 4: SRE value distributions of quantum circuits grouped by qubit number in the RQC and TIM noisy datasets are shown in Figure 4a and 4b, respectively. The M_2 values are computed under simulated noise using the IBM Fake0s1o backend.

$\theta = J\Delta t$, is realized by the standard $\text{CNOT}_{i,i+1}-\text{RZ}(2\theta)_{i+1}-\text{CNOT}_{i,i+1}$ construction, while the transverse-field term $e^{-i\phi X_i}$, with $\phi = h\Delta t$, is implemented as a single-qubit rotation $\text{RX}(2\phi)_i$. The circuits span various values of the angle parameters θ, ϕ , with the number of Trotter steps ranging in $T = [1, 5]$.

5. Graph Neural Networks for Nonstabilizerness Estimation

This section describes the proposed Graph Neural Network approach for nonstabilizerness estimation under both classification and regression problem formulations. All problem formulations share the same graph-based quantum circuit representation and GNN architecture. Figure 5 provides an overview of the whole pipeline. The proposed graph-based representation consists of two main components. The first, in yellow, is the directed acyclic graph representation of the circuit, which is encoded as an adjacency matrix together with node embeddings that represent quantum gates. The second component, in green, is the global feature set encoding the total gate count. These two components are processed independently, the first is passed through a sequence of Transformer convolutional layers, while the second through a fully connected neural network. The resulting latent representations are concatenated and passed through a regressor. Section 5.1 and Section 5.2 describe the details of the encoding technique employed and the GNN architecture, respectively.

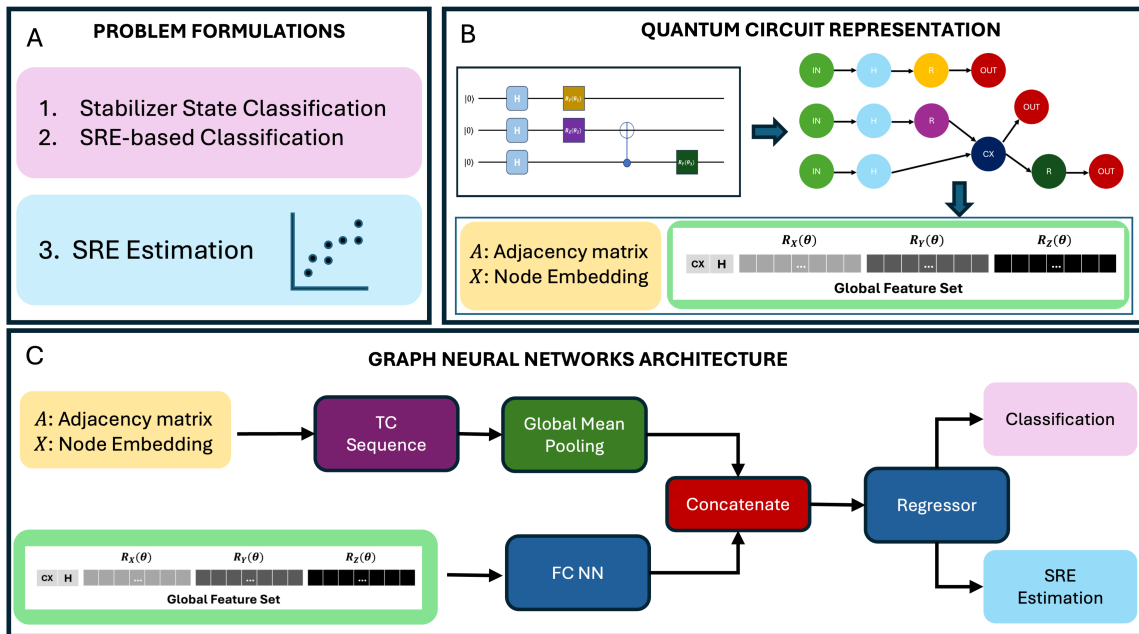


Figure 5: Overview of the GNN approach to nonstabilizerness estimation. Box A summarizes the three different problem formulations, box B illustrates the process to translate a quantum circuit in our graph-based representation, and box C illustrates the GNN architecture.

5.1. Quantum Circuit Representation

Quantum circuits can be naturally represented by directed acyclic graphs, where each node is a gate and each edge is a qubit acted upon by a gate [42, 43]. The graph passed in input to the GNN is encoded by two matrices, the adjacency matrix A representing the

graph structure, and the node feature matrix X , which contains the node embeddings. Since we deal with directed graphs, the adjacency matrix is not symmetric. Each node has an associated node embedding $x \in \mathbb{R}^d$. The size of the node embedding is $d = d_g + d_q + d_h$, as it stores the information regarding the gate type in d_g components, the target qubit(s) upon which they are applied in d_q components, and the specifics of the quantum backend in d_h components. The gate type and qubit indices are encoded using one-hot encoding, while the quantum backend vector is intrinsically real-valued. The one-hot encoding for the gate type requires $d_g = 7$ bits, one for each gate type: input gate (qubit initialization), output gate (measurement), CNOT, H, RX, RY, and RZ. The one-hot encoding for the target qubit requires a number of bits equal to the number of qubits d_q in the largest quantum circuit of the dataset. The hardware-dependent noise specifics of the gate applied require a real-valued vector of $d_h = 7$ seven components, encoding the relaxation time T_1^q , the dephasing time T_2^q and readout error r_q on the qubit(s) q on which the gate is applied, and the gate error g_ϵ . Thus, in the stabilizer state classification and the SRE-based classification, where the datasets include quantum circuits with up to 25 qubits the dimension of the node embedding is $d = 7 + 25 + 0 = 32$. In the noiseless SRE estimation task, where circuit have up to 6 qubits the embedding dimension is $d = 7 + 6 = 13$. In the noisy SRE estimation, we concatenate to the base node embedding of the noiseless case the 7-dimensional vector encoding the specifics of the IBM Fake Oslo backend, resulting in $d = 13 + 7 = 20$. Figure 5 provides a comprehensive overview on the whole pipeline, including the architecture of the model.

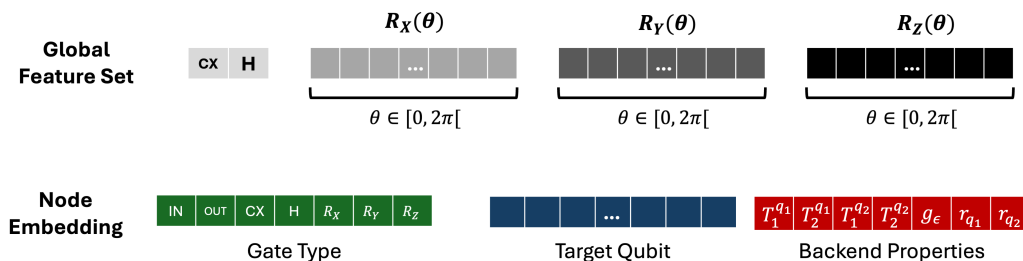


Figure 6: At the top, the global feature set, which is a vector in \mathbb{R}^d encoding the gate count. The unparameterized gates are simply counted, while the parameterized gates are first divided into 50 components, discretizing the angle parameter, and then counted. At the bottom, the (local) node embedding, which is a vector in \mathbb{R}^d encoding gates, including their type, position, and specifics related to their implementation on hardware.

The global feature set provided as input to the GNN model is a vector that encodes the gate count of quantum circuits. This representation has proven effective for supervised learning approaches to SRE estimation [25]. It consists of a vector of length 152, where unparameterized gates are directly counted, whereas parameterized gates are discretized by dividing the interval $[0, 2\pi[$ of the angle parameter into fifty equally

spaced bins. Figure 6 illustrates both the global feature set and the node embeddings of the graph-based circuit representation.

The quantum circuit representation is exactly the same for all the three formulations of the nonstabilizerness estimation problem. However, in the noisy scenario, we had to take into account the universal gate set of the IBM Fake Oslo backend. Then, we adapted the encoding on the new gate set and trained the model on the transpiled quantum circuits.

5.2. Graph Neural Network Architecture

The architecture of the Graph Neural Network employed in this work is inspired by previous works, where GNNs models are trained to predict the expressibility of quantum circuits [43] and to predict noise impact on circuit fidelity [33].

The model is divided into two main independent components. The first component processes the graph representation, including the adjacency matrix A and the node embeddings X , which are initialized as vectors encoding the gate type and target qubit(s), as described in the previous section. These are processed by three Transformer Convolutional (TC) layers that aggregate local neighborhood information within the graph. A ReLU activation function is applied between each pair of consecutive TC layers to mitigate potential numerical issues arising from negative values [43]. Finally, the resulting feature vectors, obtained after applying the sequence of TC and ReLU layers, are aggregated using global mean pooling. The second component is a fully connected artificial neural network that takes as input the global feature set, the vector encoding the gate counts of entire quantum circuits, as defined in the previous section. Finally, the output vectors from the two components are concatenated and passed through a regressor consisting of three fully connected layers interleaved with two ReLU activation layers.

However, there are key differences between the GNN implementations for the classification and regression tasks. In the stabilizer state classification setting, we use the binary cross-entropy loss function, and the output of the GNN is passed through a sigmoid function with a threshold of 0.5 to assign the class label of each quantum circuit. In contrast, for the SRE estimation problem, we employ the Huber loss function, and the final output of the GNN directly represents the predicted M_2 value of the input quantum circuit. Additionally, the circuit representations differ slightly across the various experimental configurations, as described in the previous section. Note that we employed a grid search to tune some hyperparameters of the GNN, such as the number of the TC layers, the hidden dimension of the fully connected neural networks, and the learning rate.

6. Experimental Results

This section reports the experimental setup and results conducted to assess the proposed GNN approach on three different problem formulations of increasing difficulty. Section 6.1 focuses on the stabilizer state classification task, Section 6.2 on the more challenging SRE-based classification task, and Section 6.3 on the SRE estimation task. Each section outlines the training procedure and performance evaluation by assessing the generalization capability of the proposed GNN in predicting M_2 across different scenarios. when tested on quantum circuits with a higher number of qubits, a larger total gate count, and greater entanglement levels than those used for training.

Section 6.4 investigates the sources of improvement achieved by our GNN relative to prior SVR-based approaches [25]. To this end, we evaluate the model’s performance following the ablation [47, 48] of the graph-based representation and the Transformer layers that process it, resulting in a simplified fully connected neural network trained only on the global feature set. Finally, Section 6.5 extends the SRE estimation experiments to a noisy setting, considering transpiled quantum circuits labeled by simulating the noise of an IBM quantum backend.

6.1. Stabilizer State Classification

The experiments for training and testing our GNN model on the stabilizer state classification problem can be divided into two main parts. The first part focuses on quantum circuits with a fixed number of qubits, set to 18, to allow a direct comparison with the previous approach [24]. The second part extends the experiments to a broader dataset of quantum circuits with the number of qubits ranging from 2 to 25.

In the first part of the experiments, GNN is trained on 10000 out of the 15000 circuits in PS 18, where both the training and test set are balanced between the two labels, stabilizer and magic states. Our GNN achieves a classification accuracy of 99.98% on the training set and 99.72% on the test set. When evaluated on the Clifford-evolved circuits of the dataset CS 18, the GNN accuracy keeps stable for the classification of stabilizer states, while it decreases as a function of the Clifford depth for magic states, see the blue lines in Figure 7. This phenomenon is also experienced by the CNN model. However, the classification accuracy obtained by the CNN decreases when evaluated on Clifford-evolved quantum states with Clifford depth ranging from 0 to 8. For magic states, it decreases from 100% to approximately 90%, and for stabilizer states, from 100% to 80%. In contrast, our GNN manages to maintain stable the perfect classification accuracy for stabilizer states, and for magic states the accuracy only decreases from almost 100% to 99% at depth 8. Furthermore, we extended the analysis up to a Clifford depth of 25, where the accuracy obtained by the GNN on magic states decreases to 97%, while the accuracy on the stabilizer states is still stable to 100%. We refer the reader to Figure 7.

Additionally, we extended the evaluation performance of the GNN models to other types of out-of-distribution instances. These include the circuits of the dataset ES 18,

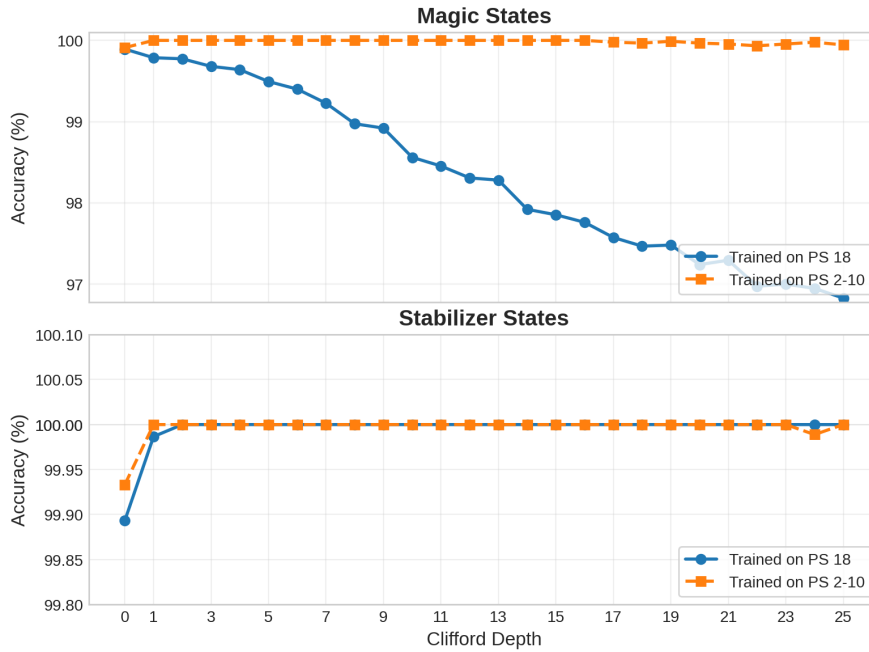


Figure 7: Stabilizer State Classification. Accuracy of the GNN model independently trained on two datasets of product states and evaluated on their corresponding Clifford-evolved datasets. The top plot shows the results for magic states, and the bottom plot shows those for stabilizer states. Results in blue correspond to the GNN trained on the 18-qubit product state dataset (PS 18), while results in orange correspond to the GNN trained on product states with a number of qubits ranging from 2 to 10.

which keep the same qubit number but with a substantially different structure, due to a high number of CNOT gates injected randomly throughout the circuits, and the circuits in the dataset PS 11-25 which are also product states as those used during training but with different number of qubits. Figure 8a illustrates the accuracy obtained by the model across the different datasets, each corresponding to testing GNN on a distinct generalization task. Specifically, PS 18 tests generalization to unseen circuits within the same dataset used for training, CS 18 evaluates generalization to circuits evolved under random Clifford gates, and ES 18 assesses generalization to circuits with higher entanglement and different structural properties.

In the second part, the GNN model is trained on circuits with low qubit numbers, specifically from 2 to 10. The training and test sets are split in a 70 to 30 ratio and kept balanced between the two classes. In this case, our GNN achieves a classification accuracy of 99.98% on the training set and 99.78% on the test set. Despite the previous case of 18-qubit circuits, the GNN manages to maintain approximately a perfect classification accuracy on both stabilizer and magic states on the subset of circuits with number of qubits between 2 and 10 of the dataset CS 2-25, as indicated by the orange line in Figure 7. The same GNN model is subsequently evaluated on different generalization tasks, following the same methodology as in the previous case. Figure 8b illustrates

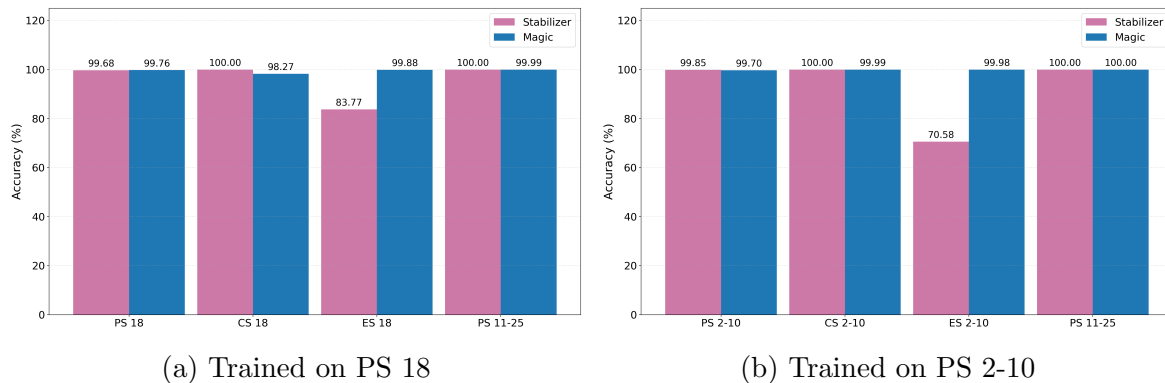


Figure 8: Evaluation of the generalization capabilities of the GNN model, in terms of classification accuracy, across different datasets for both stabilizer states (purple) and magic states (blue).

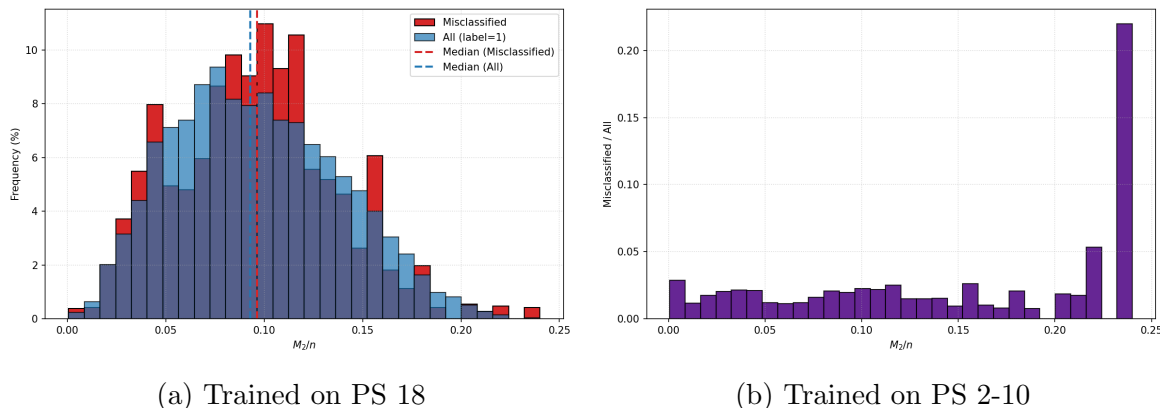


Figure 9: Evaluation of the GNN model trained on PS 18 over the circuits in CS 18 for different SRE density values (M_2/n).

the classification accuracy for both stabilizer and magic states across various datasets. Remarkably, the model successfully classifies with high accuracy the product states with higher numbers of qubits in the PS 11–25 dataset, their Clifford-evolved counterparts in the CS 2–10 dataset, and the circuit with different structure and higher level of entanglement in ES 2-10. These experimental results disclose the strong generalization performances achieved by the GNN model in the stabilizer state classification task.

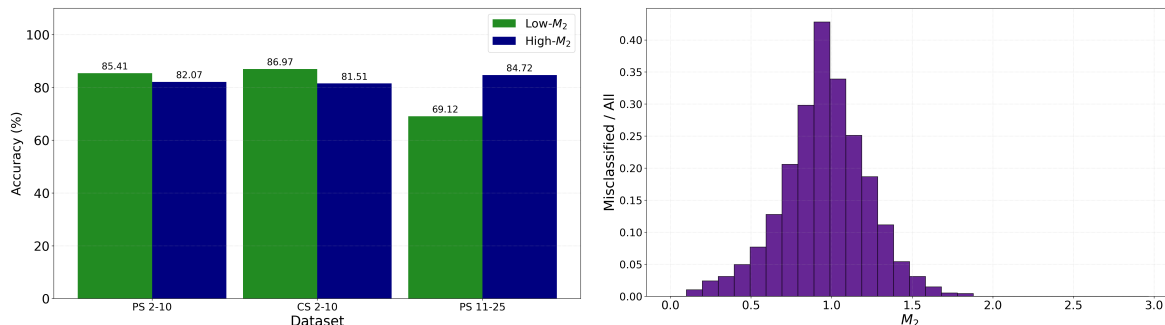
In Section 4.1 we discussed the importance of including quantum circuits with low M_2 in the datasets the classification task is easier for magic states with high M_2 density: $m_2 = M_2/n$. Figure 9 presents the results of the GNN model trained on PS 18 and evaluated on CS 18 for different values of m_2 , where we divided the range from 0 to 0.24 in 30 bins. Specifically, Figure 9a plots in red the data distribution at different ranges of m_2 compared with the distribution of the misclassified circuits from CS 18 in blue. The vertical lines represent the medians of the two distributions, which are 0.093 and 0.096, respectively. Figure 9b reports the ratio of misclassified circuits to the total

number of circuits in CS 18 for each of the 30 bins. The peak visible at the far right of the plot can be attributed to the few circuits located in the last bin, which correspond to the tail of the distribution shown in Figure 9a. In fact, in the last bin there are 11 circuits that are misclassified out of only 50 total circuits. Note that in both plots of Figure 9, we only consider the circuits labeled as magic states, which account for half of the CS 18 dataset (187500 circuits), since for all other circuits $m_2 = 0$. Overall, these experimental results indicate that the GNN classification performance remains robust across different ranges of m_2 values.

6.2. SRE-based Classification

The experiments for the SRE-based classification task follow the same procedure described for the stabilizer state classification. In this experimental setup, the GNN model is trained on product-state circuits with qubit numbers up to 10 (dataset PS 2–10), using a train–test split ratio of 70 to 30. The generalization performance is then evaluated on three different scenarios: unseen circuits from the test set, product states with a higher number of qubits (dataset PS 11–25), and Clifford-evolved circuits with depths up to 25 (dataset CS 2–10).

Figure 10 presents the experimental results of the GNN model trained for the SRE-based classification task on the PS 2–10 dataset. Figure 10a reports the classification accuracies across the three evaluation scenarios, for both low- M_2 circuits (in green) and high- M_2 circuits (in blue). Even for this more challenging classification task, the GNN achieves consistently high accuracy. Across all three scenarios, the accuracies remain above 80%, except for the case of low- M_2 circuits in the PS 11–25 dataset. In this latter dataset, the M_2 values differ substantially from those observed during training, with the maximum increasing from 3 to 5 and the median shifting from 0.90 to 1.61, as shown in the Figure 2. Figure 10b shows the ratio of circuits misclassified by the GNN



(a) Generalization across different scenarios

(b) Performance dependence on M_2

Figure 10: Evaluation of the GNN model for the SRE-based classification. On the left, the classification accuracy to evaluate the generalization performances across different scenarios. On the right, a study on the performance of the GNN model depending on M_2 .

to the total number of circuits in the dataset, plotted as a function of their M_2 values. The plot exhibits a Gaussian-like distribution centered around the M_2 threshold (0.90). This behavior is expected, as the classification task becomes increasingly challenging for circuits with M_2 values close to the threshold, where distinguishing between low- and high- M_2 circuits is inherently more difficult. We note that in the previous section we provide a study on the performance depending on m_2 , as it was a specific case of fixed qubit number addressed to compare with previous work. In this more general case, is the M_2 value of the whole circuit that matter.

Figure 11 provides a detailed analysis of the classification accuracy achieved by the GNN on the Clifford-evolved datasets as a function of Clifford depth. For this analysis, we additionally trained the GNN on the PS 2–25 dataset to study how the model performance scales with the problem size. The blue curves correspond to the accuracies obtained by the GNN trained on PS 2–10 and evaluated on CS 2–10, while the orange curves represent the results of the GNN trained on the larger PS 2–25 dataset and evaluated on CS 2–25. The top plot reports the accuracies for high- M_2 quantum circuits, whereas the bottom plot shows the accuracies for low- M_2 circuits. Interestingly, scaling up the problem reveals a distinct behavior. For high- M_2 circuits, the accuracy achieved on smaller systems (2–10 qubits) remains more robust under Clifford evolution compared to the more challenging case with 11–25 qubits. Conversely, for low- M_2 circuits, while the accuracy decreases with Clifford depth in the smaller-qubit case, it

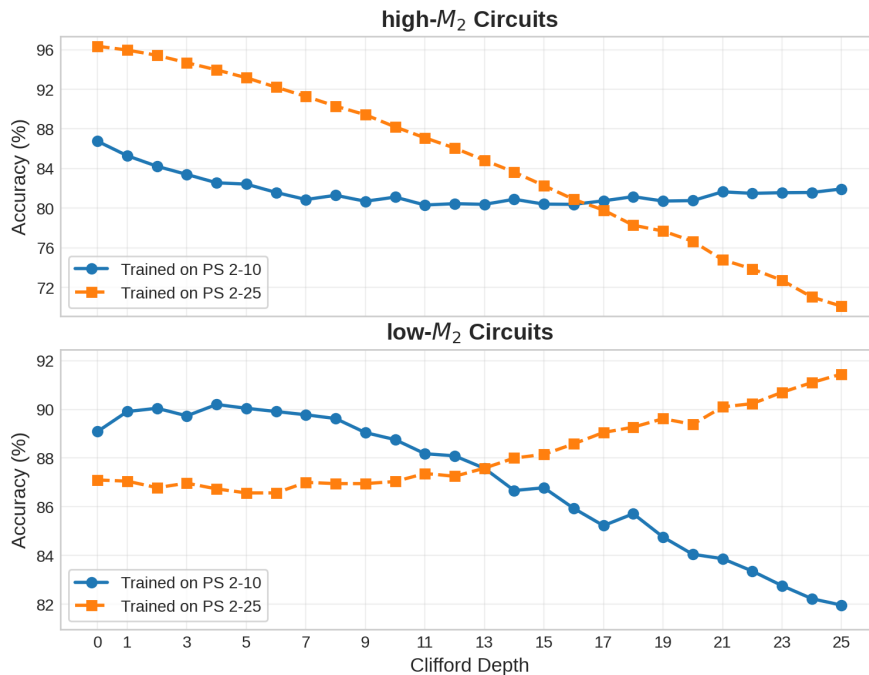


Figure 11: Accuracy of the GNN model for the SRE-based classification task. The GNN is independently trained on two datasets of product states and evaluated on their corresponding Clifford-evolved datasets.

improves for the larger one. It is important to note that all circuits in the datasets contain both Clifford and non-Clifford gates. As the Clifford depth increases, not only does the circuit structure change, but also the ratio of Clifford to non-Clifford gates grows. Furthermore, the larger PS 2–25 dataset offers greater variance and a larger sample size, which contribute to the model’s improved generalization behavior. The improvement in the accuracy might be the sign that our GNN model managed to capture this structural feature.

6.3. Stabilizer Rényi Entropy Estimation

The experiments for training and testing our GNN model for SRE estimation are aligned with the setting proposed in [25]. The experiments can be divided into two main parts. The first part is designed to evaluate the generalization capabilities of GNN in terms of number of qubits, while the second in terms of circuit depth.

To assess the generalization capabilities of our GNN approach, we test its performance on out-of-distribution instances. In particular, we evaluate how the GNN generalizes with respect to the number of qubits and the gate counts. We refer to these experiments as *extrapolation* in qubit number and in gate count, respectively. We train our GNN independently on the two quantum circuits datasets, RQC and TIM. In all experiments we split training and test set in 80-20. Note that, to ensure statistical robustness, each experiment is repeated ten times with different random seeds, and the reported results correspond to the average results over these ten independent runs.

Figure 12 summarizes the experiments designed to test the extrapolation in the qubit number. Here, the models are trained on the subset of quantum circuits with qubit numbers from 2 to 5, and then evaluated on 6-qubit circuits. The difference between the MSE values obtained by the SVR on the training and test set suggests the presence of overfitting. This effect is observed in both datasets. In the RQC dataset, the MSE increases from 0.175 on the training set to 0.202 on the test set, while in the TIM dataset, the MSE increases from 0.22 to 0.25. As a result, the generalization performances are limited as the MSE increases of approximately of a factor 3.5 in the RQC dataset and 4.5 in the TIM dataset. In contrast, the GNN model significantly improves upon the results obtained with SVR, particularly in terms of Mean Squared Error (MSE) on the extrapolation set. Specifically, GNN reduces the extrapolation MSE upon SVR by the 79% on RQC, and by 26% on TIM. The highest improvement is achieved on the RQC dataset, where the GNN also reduces the gap between the MSE values obtained on the training and test set.

Figure 13 summarizes the experiments designed to test the extrapolation in gate counts. Here, the models are trained on the subset of circuits with gate counts restricted to the range $[0, 79]$ for the RQC dataset and evaluated on circuits with gate counts ranging in $[80, 99]$. This approach is similarly applied to the TIM dataset, where the model is trained on circuits with trotter steps from 1 to 4 and tested on trotter step 5. The difference between the MSE values obtained by the SVR on the training and

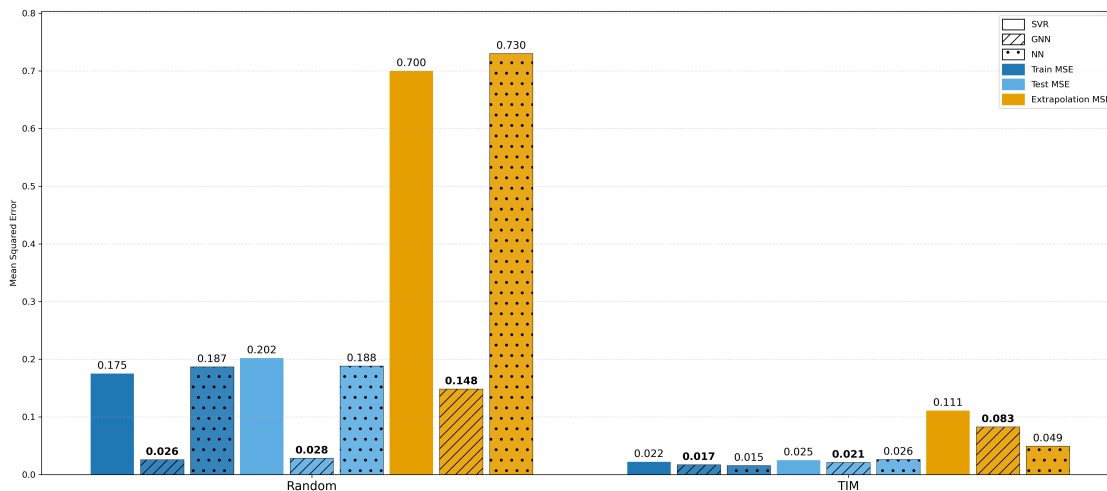


Figure 12: Performance comparison between GNN, SVR (hatched), and NNs (dotted) in the setup of extrapolation per qubit number.

test sets indicates a slight overfitting effect. This behavior is more evident on the RQC dataset, where the MSE increases from 0.189 in the training set to 0.219 in the test set. In contrast, for the TIM dataset, the MSE increases only from 0.26 to 0.28, resulting in a slightly better generalization performance compared to the RQC dataset. In this setting, our GNN demonstrates strong generalization performance. The gap between training and test MSE observed in the SVR model for the RQC dataset is reduced, and concurrently the extrapolation MSE improves by 95%, from 0.532 to 0.025. Moreover, the GNN achieves an extrapolation MSE of 0.028, which improves the SVR model by 56%. Table 3 summarizes the results obtained in terms of MSE on the extrapolation set compared to the Support Vector Regressor proposed in [25]. In addition, it includes the results obtained by training a Neural Network as described in Section 6.4.

It is important to focus on the extrapolation MSE obtained on the RQC dataset when extrapolating on gate counts, as it is unexpectedly lower than the training MSE. However, Figure 3c shows that the SRE distribution of the quantum circuits in RQC becomes narrower, with the standard deviation decreasing as the gate count increases. Since M_2 is bounded above by $SRE_{max}(n) = \ln(\frac{2^n+1}{2})$ [10], for a quantum system of n qubits, higher gate counts that include non-Clifford gates drive the system towards a more stable regime with smaller variance. To further investigate this effect, we perform an additional experiment in which we train our GNN on quantum circuits with the largest gate counts, namely from 20 to 99, and extrapolate on the shallower circuits with gate counts from 1 to 19. In this setup, we require the model to extrapolate on a subset of circuits with a wider interval of M_2 , higher standard deviation, and less separation. As a result, extrapolating in the new setup should be more difficult. Figure 14 presents a direct comparison between two extrapolation experiments. The bars on the left, relate to the GNN extrapolation on higher gate counts. On the right, there are the bars related to the extrapolation to unseen circuits with lower gate counts.

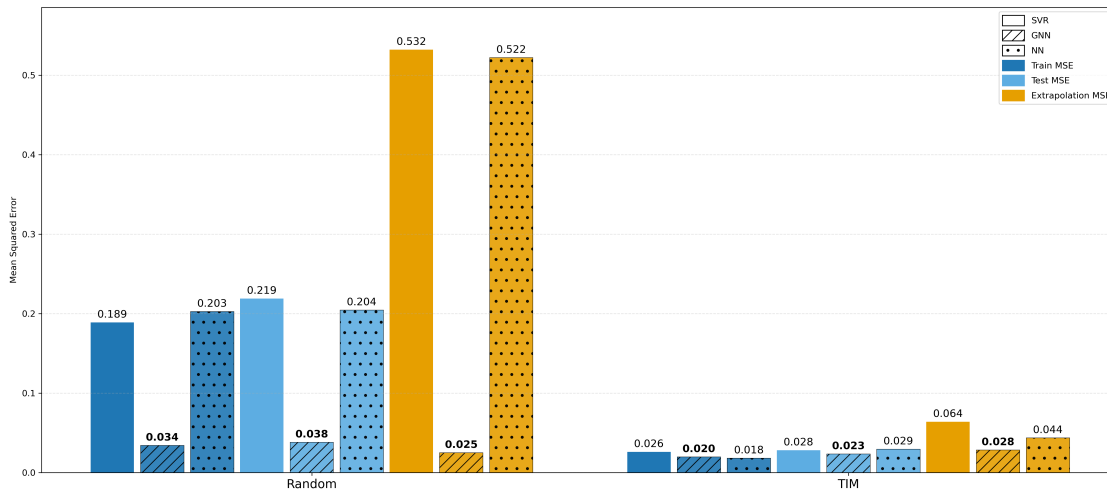


Figure 13: Performance comparison between GNN, SVR (hatched), and NNs (dotted) in the setup of extrapolation per gate count.

As expected, the extrapolation MSE in the latter setting is higher than in the former, and also exceeds the training MSE.

6.4. The Importance of the Graph Representation

Given the improved performance of the GNN compared to the SVR model, it is important to investigate the source of this advantage. We identify two main differences between the GNN and SVR approaches. First, the GNN employs a graph-based representation combined with Transformer Convolutional layers, which aggregate local information from neighboring nodes. Second, the GNN leverages a deep learning architecture to process the global feature set, which is the same set used in the SVR model [25].

To examine the importance of the graph representation, we perform experiments by isolating the fully-connected neural network from the upper part of the model shown in Figure 5. This is a common process in artificial intelligence, known as ablation, where an individual component is obscured in order to evaluate its contributions to the whole complex models [47, 48]. In this setup, we disabled the Transformers Convolutional

Table 3: Relative performance of the GNN and NN models compared to the SVR baseline [25], in terms of the extrapolation MSE.

Extrapolation on Qubit Number

Dataset	GNN	NN
RQC	-78.8%	+4.3%
TIM	-25.6%	-55.6%

Extrapolation on Gate Counts

Dataset	GNN	NN
RQC	-95.3%	-1.9%
TIM	-55.6%	-31.6%

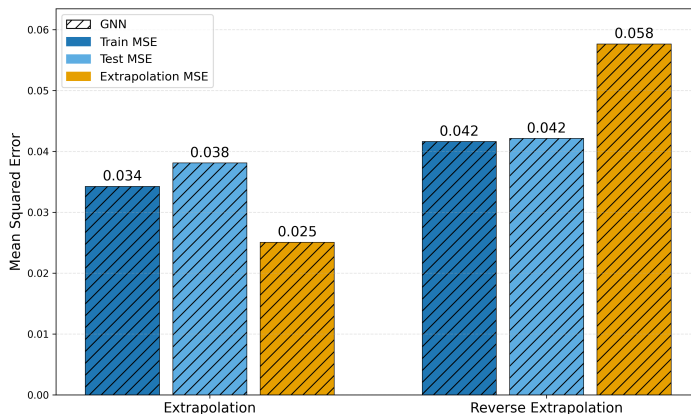


Figure 14: Extrapolation performance of the GNN model with respect to gate counts in the RQC dataset. On the left, the bars correspond to the canonical extrapolation on larger circuits, while on the right, they correspond to the extrapolation on smaller circuits.

responsible for processing the graph-structured data. Consequently, we train only the fully connected neural network (NNs) on the global feature set. The dotted bars in Figure 12 and Figure 13 show the results obtained in this experimental setup for the extrapolation on qubit number and gate count, respectively. Table 3 compares directly the extrapolation performances of GNN and NN with respect to the SVR model [25].

The experiments show that the graph representation has a significant impact on the SRE estimation problem in the RQC dataset. In the case of extrapolation on the qubit number, the 79% improvement in MSE over SVR completely vanishes when training only a neural network on the global feature set, and performance even degrades, becoming 4% worse than SVR. Similarly, for extrapolation on gate counts, the 95% improvement in GNN vanishes to approximately 2%. However, on the TIM dataset, the impact of the graph representation is different. While NN loses nearly half of the advantage gained by the GNN (achieving a 33% improvement compared to the 56% for the GNN) in extrapolating on gate counts, the NN achieves a significantly better result than the GNN when extrapolating on the qubit number (56% versus 26% for the GNN). These experimental results suggest that the circuit structure has the highest impact on the datasets where there is more diversity. In this regard, the RQC dataset is composed of random quantum circuits with different structure, while the TIM dataset has a structure of a fixed sequence of gates that repeats on different combination of qubits and with the diversity hidden in the angle parameters of the rotation gates.

6.5. Quantum Noise Effect on Stabilizer Rényi Entropy Estimation

One of the main motivations for adopting the Stabilizer Rényi Entropy (SRE) as a measure of nonstabilizerness in this work is its suitability for experiments on real quantum devices [13, 14]. For this reason, in this section we assess the impact of

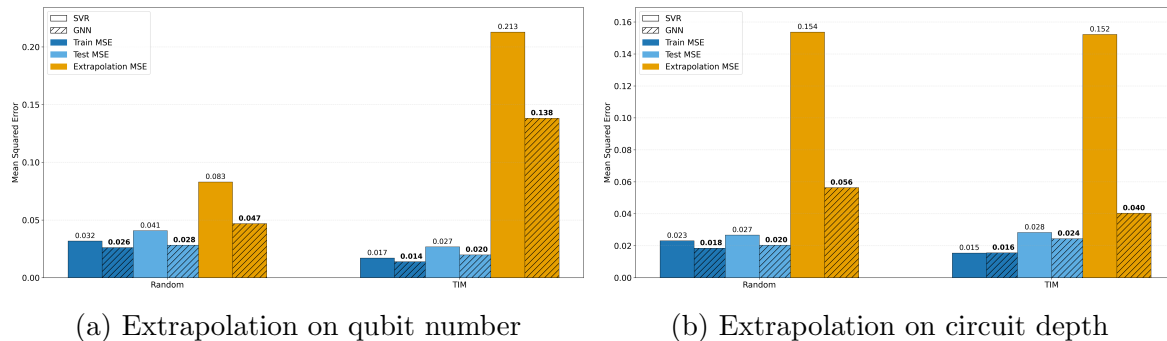


Figure 15: Comparison between GNN and SVR (hatched) in terms of MSE on the RQC Noisy and the TIM Noisy datasets.

quantum noise on the predictions of our GNN models. The RQC Noisy and TIM Noisy datasets have been generated specifically for this task. In these datasets, all quantum circuits are labeled with their M_2 values obtained by simulating quantum noise using the IBM Fake Oslo backend.

The experiments in this setup follow exactly the same procedure as those described in Section 6.3. Figure 15 reports the mean squared error (MSE) values for the extrapolation experiments with respect to the qubit number (Figure 15a) and the gate count (Figure 15b). The SVR model was trained following the procedure described in [25], including a grid search over the hyperparameters.

We note that the noisy RQC and TIM datasets are smaller in size compared to their respective noiseless counterparts, given the high computational time required for their simulation. For this reason, a comparison of the results between the model predictions obtained in the noisy and noiseless scenarios has to be interpreted with caution, as part of the performance gap may be attributed to the reduced training set size rather than the effect of noise itself.

7. Conclusions

This article proposed a Graph Neural Network (GNN) approach for addressing the nonstabilizerness estimation problem in the supervised learning setting through three formulations of increasing difficulty. The first is the stabilizer state classification, which is defined independently of any specific nonstabilizerness measure. This formulation serves primarily as a benchmark to establish a consistent data generation procedure and to perform an initial assessment of the GNN model on an easier problem. The second is the SRE-based classification defined on the stabilizer Rényi entropy (SRE). This formulation represents a more challenging and physically motivated task, as it directly connects to identifying stabilizer states based on their SRE measured on a real quantum device. Finally, the SRE estimation, is the more general regression task, which aims to predict the SRE of quantum circuits as a quantitative measure of nonstabilizerness [49].

In the first two classification tasks, the GNN model is trained on product-state

quantum circuits. Compared to previous CNN-based approaches [24], the proposed GNN model achieves more robust generalization performance on circuits evolved under Clifford operations. Since the CNOT is a Clifford gate, Clifford-evolved circuits allow to test the generalization capabilities to entangled states. Our proposed data generation procedure includes not only stabilizer and highly magic states but also quantum states with low SRE values. This diversity is a fundamental feature of the dataset, as it prevents the problem from being defined on states that are easily separable. Additionally, we extended the analysis to circuits with different structure and high number of CNOT gates, as well as on circuits with higher number of qubits, where the GNN also exhibits robust performances. For the regression task, our GNN model provides more accurate SRE predictions than the Support Vector Regressor [25], especially in terms of generalization to larger, previously unseen quantum circuits. By ablation of the graph representation and the GNN components that process the graph data, we show that the graph representation improves the model predictions. The impact of the graph representation is significantly relevant on random quantum circuit where circuit structures are quite different. Moreover, the experimental results show that the proposed GNN is a promising approach to predict SRE values measured on a given hardware platform. This is because the graph-based framework effectively accommodates the backend information of quantum devices. However, more extensive experiments involving tests on different quantum devices and noise models are necessary to thoroughly assess the capability of our GNN to predict the noisy SRE measurements on real quantum devices. To facilitate benchmarking and support advancements in this field, we release a comprehensive dataset of quantum circuits specifically designed for the nonstabilizerness estimation problem in those three formulations.

The performance analysis on the experimental demonstrate that by leveraging the graph-based representation of quantum circuits, the proposed GNN model achieves accurate nonstabilizerness estimation with robust generalization capabilities to larger quantum circuits, in terms of both number of quantum circuits and gate count, and to higher entanglement. We conclude that the proposed GNN model offers an effective and scalable framework for estimating nonstabilizerness across both noiseless and noisy regimes.

Future Directions

We identify three main future research directions. The first regards the design of different features that can improve the graph-based quantum circuit representation for our GNN model. The integration of expectation values of local observables, which can be calculated efficiently through the classical shadows protocol [44], can be an interesting direction as suggested by previous theoretical [24] and experimental results [25].

The second future research direction is extending our GNN model to predict different properties of quantum circuits, such as different entropy measures, expectation values over Pauli strings, and relevant observables like Hamiltonians of quantum

systems. In this regard, performing a task-agnostic pretraining of the GNN model on our proposed dataset may enable GNN to capture general structural and statistical features of quantum circuits before undergoing problem-dependent finetuning. Pretraining would not only broaden the range of potential applications but also substantially reduce the computational cost associated with training task-specific GNN models.

The third future direction is the integration of the proposed GNN model within Quantum Architecture Search (QAS) frameworks, to enable the development of SRE-informed QAS techniques [50, 51]. A particularly suitable framework to embed SRE estimation in quantum architecture search is Monte Carlo Tree Search [49], where the information regarding the nonstabilizerness can be used in the selection or expansion steps to push the search towards quantum circuits difficult to simulate on a classical device. This direction might be significantly beneficial in the quest for achieving quantum advantage with variational quantum algorithms (VQAs) [29], as it would allow the design of quantum circuits that optimize both the quality of the solution to a target problem and their complexity in terms of classical simulation. Moreover, as evaluating objective functions in QAS requires typically significant computational effort, the proposed GNN can be used as a surrogate model to approximate these objectives. Such integration would enhance QAS efficiency and aligns with the pretraining framework described in the second future direction.

Data Availability

The data and code to reproduce the experiments described in the article are publicly available at Zenodo [27] and GitHub: https://github.com/VincenzoLipardi/GNN_SRE.

Acknowledgments

The authors acknowledge the financial support of the Quantum Software Consortium, which facilitated the development of this work and strengthened collaborations through a visitor travel grant.

Conflict of Interests

The authors declare no conflict of interests.

References

- [1] Sergey Bravyi and Alexei Kitaev. Universal quantum computation with ideal clifford gates and noisy ancillas. *Phys. Rev. A*, 71:022316, Feb 2005. doi: 10.1103/PhysRevA.71.022316.

- [2] Earl T Campbell, Barbara M Terhal, and Christophe Vuillot. Roads towards fault-tolerant universal quantum computation. *Nature*, 549(7671):172–179, 2017.
- [3] Daniel Gottesman. The heisenberg representation of quantum computers. *arXiv preprint quant-ph/9807006*, 1998.
- [4] Scott Aaronson and Daniel Gottesman. Improved simulation of stabilizer circuits. *Physical Review A—Atomic, Molecular, and Optical Physics*, 70(5):052328, 2004.
- [5] Victor Veitch, Christopher Ferrie, David Gross, and Joseph Emerson. Negative quasi-probability as a resource for quantum computation. *New Journal of Physics*, 14(11):113011, 2012.
- [6] Mark Howard and Earl Campbell. Application of a resource theory for magic states to fault-tolerant quantum computing. *Physical review letters*, 118(9):090501, 2017.
- [7] Markus Heinrich and David Gross. Robustness of magic and symmetries of the stabiliser polytope. *Quantum*, 3:132, 2019.
- [8] Michael Beverland, Earl Campbell, Mark Howard, and Vadym Kliuchnikov. Lower bounds on the non-clifford resources for quantum computations. *Quantum Science and Technology*, 5(3):035009, 2020.
- [9] Tobias Haug and MS Kim. Scalable measures of magic resource for quantum computers. *PRX Quantum*, 4(1):010301, 2023.
- [10] Lorenzo Leone, Salvatore FE Oliviero, and Alioscia Hamma. Stabilizer rényi entropy. *Physical Review Letters*, 128(5):050402, 2022.
- [11] Lorenzo Leone and Lennart Bittel. Stabilizer entropies are monotones for magic-state resource theory. *Physical Review A*, 110(4):L040403, 2024.
- [12] Arash Ahmadi and Eliska Greplova. Quantifying non-stabilizerness via information scrambling. *SciPost Physics*, 16(2):043, 2024.
- [13] Salvatore FE Oliviero, Lorenzo Leone, Alioscia Hamma, and Seth Lloyd. Measuring magic on a quantum processor. *npj Quantum Information*, 8(1):148, 2022.
- [14] Pradeep Niroula, Christopher David White, Qingfeng Wang, Sonika Johri, Daiwei Zhu, Christopher Monroe, Crystal Noel, and Michael J Gullans. Phase transition in magic with random quantum circuits. *Nature Physics*, 20(11):1786–1792, 2024.
- [15] Tobias Haug and Lorenzo Piroli. Quantifying nonstabilizerness of matrix product states. *Physical Review B*, 107(3):035148, 2023.
- [16] Poetri Sonya Tarabunga, Emanuele Tirrito, Mari Carmen Bañuls, and Marcello Dalmonte. Nonstabilizerness via matrix product states in the pauli basis. *Physical Review Letters*, 133(1):010601, 2024.
- [17] Poetri Sonya Tarabunga, Emanuele Tirrito, Titas Chanda, and Marcello Dalmonte. Many-body magic via pauli-markov chains—from criticality to gauge theories. *PRX Quantum*, 4(4):040317, 2023.
- [18] Guglielmo Lami and Mario Collura. Nonstabilizerness via perfect pauli sampling of matrix product states. *Physical Review Letters*, 131(18):180401, 2023.

- [19] Guglielmo Lami and Mario Collura. Unveiling the stabilizer group of a matrix product state. *Physical Review Letters*, 133(1):010602, 2024.
- [20] Alessandro Sinibaldi, Antonio Francesco Mello, Mario Collura, and Giuseppe Carleo. Non-stabilizerness of neural quantum states. *arXiv preprint arXiv:2502.09725*, 2025.
- [21] Giuseppe Carleo, Ignacio Cirac, Kyle Cranmer, Laurent Daudet, Maria Schuld, Naftali Tishby, Leslie Vogt-Maranto, and Lenka Zdeborová. Machine learning and the physical sciences. *Reviews of Modern Physics*, 91(4):045002, 2019.
- [22] Vedran Dunjko and Hans J Briegel. Machine learning & artificial intelligence in the quantum domain: a review of recent progress. *Reports on Progress in Physics*, 81(7):074001, 2018.
- [23] Mario Krenn, Jonas Landgraf, Thomas Foesel, and Florian Marquardt. Artificial intelligence and machine learning for quantum technologies. *Physical Review A*, 107(1):010101, 2023.
- [24] Antonio Francesco Mello, Guglielmo Lami, and Mario Collura. Retrieving nonstabilizerness with neural networks. *Phys. Rev. A*, 111:012440, 2025.
- [25] Vincenzo Lipardi, Domenica Dibenedetto, Georgios Stamoulis, and Mark HM Winands. A study on stabilizer rényi entropy estimation using machine learning. *arXiv preprint arXiv:2509.16799 (Accepted for publication in the Proceedings of the IEEE International Conference on Quantum Artificial Intelligence 2025)*, 2025.
- [26] Franco Scarselli, Marco Gori, Ah Chung Tsoi, Markus Hagenbuchner, and Gabriele Monfardini. The graph neural network model. *IEEE transactions on neural networks*, 20(1):61–80, 2008.
- [27] Vincenzo Lipardi. Quantum circuit dataset for nonstabilizerness estimation, 2025. doi:10.5281/zenodo.17735525.
- [28] Michael A Nielsen and Isaac L Chuang. *Quantum computation and quantum information*. Cambridge University Press, 2010.
- [29] Marco Cerezo, Andrew Arrasmith, Ryan Babbush, Simon C Benjamin, Suguru Endo, Keisuke Fujii, Jarrod R McClean, Kosuke Mitarai, Xiao Yuan, Lukasz Cincio, et al. Variational quantum algorithms. *Nature Reviews Physics*, 3(9):625–644, 2021.
- [30] Thomas Spriggs, Arash Ahmadi, Bokai Chen, and Eliska Greplova. Quantum resources of quantum and classical variational methods. *Machine Learning: Science and Technology*, 6(1):015042, 2025.
- [31] Nadish de Silva, Wilfred Salmon, and Ming Yin. Fast algorithms for classical specifications of stabiliser states and clifford gates. *Quantum*, 9:1586, 2025.
- [32] Xiaoqian Zhang, Maolin Luo, Zhaodi Wen, Qin Feng, Shengshi Pang, Weiqi Luo, and Xiaoqi Zhou. Direct fidelity estimation of quantum states using machine learning. *Physical Review Letters*, 127(13):130503, 2021.
- [33] Hanrui Wang, Zhiding Liang, Jiaqi Gu, Zirui Li, Yongshan Ding, Weiwen Jiang, Yiyu Shi, David Z Pan, Frederic T Chong, and Song Han. Torchquantum case study

- for robust quantum circuits. In *Proceedings of the 41st IEEE/ACM International Conference on Computer-Aided Design*, pages 1–9, 2022.
- [34] Vedika Saravanan and Samah M Saeed. Data-driven reliability models of quantum circuit: From traditional ml to graph neural network. *IEEE Transactions on Computer-Aided Design of Integrated Circuits and Systems*, 42(5):1477–1489, 2022.
- [35] Avi Vadali, Rutuja Kshirsagar, Prasanth Shyamsundar, and Gabriel N Perdue. Quantum circuit fidelity estimation using machine learning. *Quantum Machine Intelligence*, 6(1):1, 2024.
- [36] Giovanni Acampora and Roberto Schiattarella. Deep neural networks for quantum circuit mapping. *Neural Computing and Applications*, 33(20):13723–13743, 2021.
- [37] Alexander Zlokapa and Alexandru Gheorghiu. A deep learning model for noise prediction on near-term quantum devices. *arXiv preprint arXiv:2005.10811*, 2020.
- [38] Yuan-Hang Zhang, Pei-Lin Zheng, Yi Zhang, and Dong-Ling Deng. Topological quantum compiling with reinforcement learning. *Physical Review Letters*, 125(17):170501, 2020.
- [39] Hongxiang Fan, Ce Guo, and Wayne Luk. Optimizing quantum circuit placement via machine learning. In *Proceedings of the 59th ACM/IEEE Design Automation Conference*, pages 19–24, 2022.
- [40] Francisco JR Ruiz, Tuomas Laakkonen, Johannes Bausch, Matej Balog, Mohammadamin Barekatin, Francisco JH Heras, Alexander Novikov, Nathan Fitzpatrick, Bernardino Romera-Paredes, John van de Wetering, et al. Quantum circuit optimization with alphasolver. *Nature Machine Intelligence*, pages 1–12, 2025.
- [41] Laura Lewis, Hsin-Yuan Huang, Viet T Tran, Sebastian Lehner, Richard Kueng, and John Preskill. Improved machine learning algorithm for predicting ground state properties. *Nature Communications*, 15(1):895, 2024.
- [42] Haoran Liao, Derek S Wang, Iskandar Sitdikov, Ciro Salcedo, Alireza Seif, and Zlatko K Minev. Machine learning for practical quantum error mitigation. *Nature Machine Intelligence*, pages 1–9, 2024.
- [43] Shamminuj Aktar, Andreas Bärtzchi, Diane Oyen, Stephan Eidenbenz, and Abdel-Hameed A Badawy. Graph neural networks for parameterized quantum circuits expressibility estimation. In *2024 IEEE International Conference on Quantum Computing and Engineering (QCE)*, volume 1, pages 1547–1557. IEEE, 2024.
- [44] Hsin-Yuan Huang, Richard Kueng, and John Preskill. Predicting many properties of a quantum system from very few measurements. *Nature Physics*, 16(10):1050–1057, 2020.
- [45] John Preskill. Quantum computing in the nisq era and beyond. *Quantum*, 2:79, 2018.
- [46] Salvatore FE Oliviero, Lorenzo Leone, and Alioscia Hamma. Magic-state resource

- theory for the ground state of the transverse-field ising model. *Physical Review A*, 106(4):042426, 2022.
- [47] Paul R Cohen and Adele E Howe. How evaluation guides ai research: The message still counts more than the medium. *AI magazine*, 9(4):35–35, 1988.
- [48] Allen Newell. A tutorial on speech understanding systems. In *Speech recognition: Invited papers presented at the 1974 IEEE Symposium*, pages 3–54. Academic Press, 1975.
- [49] Vincenzo Lipardi, Domenica Dibenedetto, Georgios Stamoulis, and Mark HM Winands. Quantum circuit design using a progressive widening enhanced monte carlo tree search. *Advanced Quantum Technologies*, page e2500093, 2025.
- [50] Yuxuan Du, Tao Huang, Shan You, Min-Hsiu Hsieh, and Dacheng Tao. Quantum circuit architecture search for variational quantum algorithms. *npj Quantum Information*, 8(1):62, 2022.
- [51] Shi-Xin Zhang, Chang-Yu Hsieh, Shengyu Zhang, and Hong Yao. Differentiable quantum architecture search. *Quantum Science and Technology*, 7(4):045023, 2022.